BIOCHEMISTRY

 Volume 43, Number 51 December 28, 2004

Articles

Solution Structure, Backbone Dynamics, and Association Behavior of the C-Terminal BRCT Domain from the Breast Cancer-Associated Protein BRCA1[†,‡]

Olaf J. Gaiser,[§,||] Linda J. Ball,[*,||,@] Peter Schmieder,[||] Dietmar Leitner,[||] Holger Strauss,[||] Martin Wahl,[||] Ronald Kühne,[||] Hartmut Oschkinat,[||] and Udo Heinemann[§,⊥]

Max Delbrück Center for Molecular Medicine, Robert-Rössle-Strasse 10, D-13125 Berlin, Germany, Research Institute for Molecular Pharmacology, Robert-Rössle-Strasse 10, D-13125 Berlin, Germany, and Institut für Chemie/Kristallographie, Freie Universität, Takustrasse 6, D-14195 Berlin, Germany

Received March 6, 2004; Revised Manuscript Received July 13, 2004

ABSTRACT: BRCA1 is a tumor suppressor protein associated with breast and ovarian cancer. The C-terminal region of BRCA1 consists of two closely spaced BRCT domains which mediate essential biological functions, including regulation of transcription and control of cell-cycle progression by their interaction with phosphorylated effector proteins. Here we report the NMR structure of the isolated C-terminal BRCT domain (BRCT-c) from human BRCA1. BRCT-c is well-structured in solution, folding independently in the absence of its BRCT-n counterpart. Ultracentrifugation experiments and size exclusion chromatography reveal that BRCT-c exists as a monomer under near-physiological conditions. Dynamics measurements from NMR data show three loops which coincide with the most variable sequence regions in BRCT domains, to be genuinely flexible in solution. The solution structure of BRCT-c shows subtle conformational changes when compared to the crystal structure of BRCT-c in the tandem repeat of BRCA1. These affect sites involved in formation of the BRCT-n−BRCT-c interface and the binding to phosphoserine-containing peptides. The results suggest that the presence of native BRCT-n and a properly aligned BRCT-n−BRCT-c interface are essential if BRCT-c is to adopt a biologically active conformation. Structural consequences of cancer-associated mutations and biological implications of the dynamic behavior are discussed.

The tumor suppressor protein BRCA1[1] regulates cell growth and proliferation in breast and ovarian epithelial cells. The C-terminal region of BRCA1 includes two successive BRCT domains separated by a 23-amino acid linker (Figure 1A). BRCT domains, in different copy numbers, have been found in proteins from all biological kingdoms (*1*, *2*). These include the p53-binding protein 53BP1, Crb2, the proto-oncoprotein ECT2**,** the DNA-repair protein XRCC1, the yeast DNA-repair and cell-cycle checkpoint proteins

[†] This work was supported by the German Ministry for Education and Research (BMBF) through the Leitprojekteverbund Proteinstrukturfabrik and the Fonds der Chemischen Industrie.

[‡] Coordinates were deposited in the Protein Data Bank, as entry 1OQA.

* To whom correspondence should be addressed [E-mail: linda.ball@sgc.ox.ac.uk. Fax: ++44 1865 737231.].

[§] Max Delbrück Center for Molecular Medicine.

[||] Research Institute for Molecular Pharmacology.

[⊥] Freie Universität, Berlin.

[@] Present address: Structural Genomics Consortium, University of Oxford, Botnar Research Centre, Oxford OX37LD, U.K.

[1] Abbreviations: BRCA1, product of the *BRCA1* gene, breast and ovarian cancer susceptibility gene 1; BRCT, BRCA1 C-terminal domain; IPTG, isopropyl β-D-thiogalactopyranoside; GST, glutathione *S*-transferase; NMR, nuclear magnetic resonance; HSQC, heteronuclear single-quantum correlation spectroscopy; CSP, chemical shift perturbation.

10.1021/bi049550q CCC: $27.50
Published on Web 12/04/2004

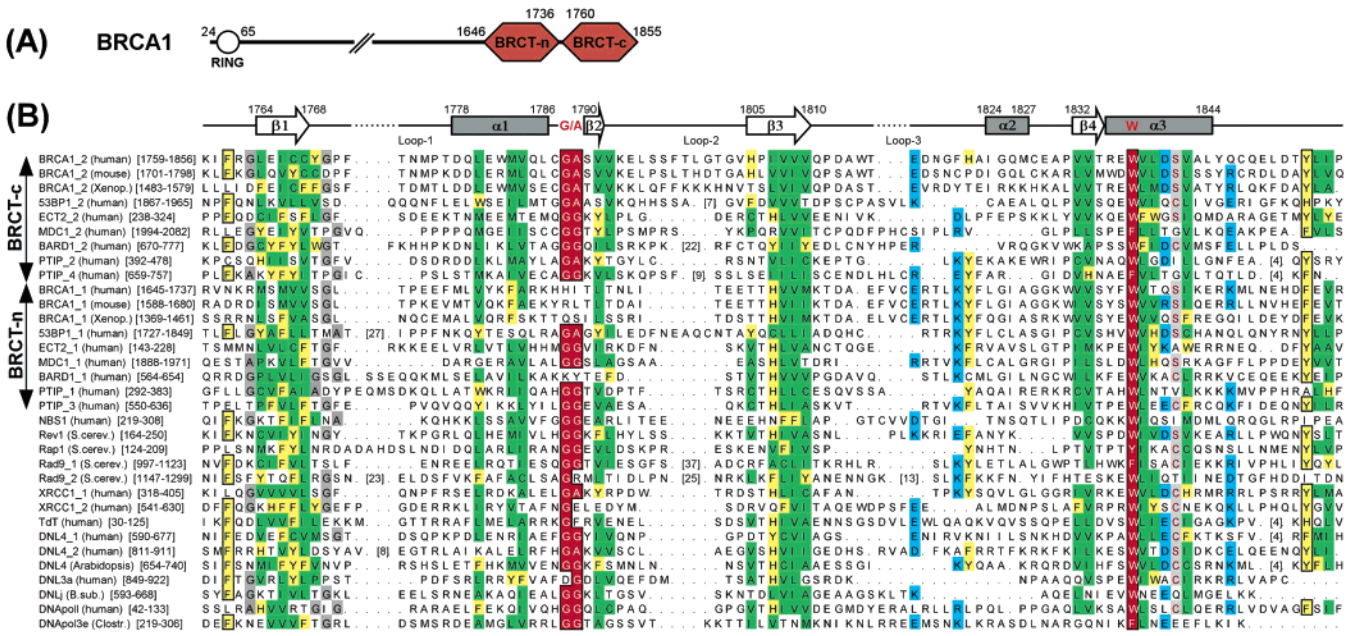

FIGURE 1: Sequence alignment of BRCT domains. (A) Domain organization in human BRCA1 (1863 residues). Residue numbers refer to the domain boundaries. RING denotes the ring finger domain; BRCT-n and BRCT-c denote the amino- and carboxy-terminal BRCT domains, respectively. (B) Selected subsets of proteins belonging to the BRCT protein family. β-Strands and α-helices as found in BRCT-c of BRCA1 are represented by arrows and cylinders, respectively, with the corresponding sequence positions denoted above. The amino acid numbers at the beginning and end of each aligned sequence are given in square brackets as well as the numbers of intervening residues between more conserved regions of the sequence. The positions of the most conserved residues, Gly1788 and Ala1789 (preceding β2) and Trp1837 (α3), are highlighted in red; other conserved residues are colored yellow (aromatic), green (aliphatic), blue (charged), gray (Gly/Ala), and brown (Cys/Ser, position 1841). In addition, the aromatic key residues (Phe1761, Trp1837, and Tyr1853 in BRCA1 BRCT-c; see also Figure 2A) and the conserved Gly/Ala cluster (positions 1788 and 1789) are boxed. BRCA1 orthologs and other proteins with BRCT tandem repeats containing BRCT-n and BRCT-c are listed first and DNA-modifying enzymes at the end. Swiss-Prot accession codes are as follows: BRCA1 (breast cancer susceptibility protein 1), P38398; 53BP1 (tumor suppressor p53-binding protein 1), Q12888; ECT2 (epithelial cell-transforming sequence 2 oncoprotein), Q9H8V3; MDC1 (mediator of DNA damage checkpoint protein 1), Q14676; BARD1 (BRCA1-associated RING domain protein), Q99728; PTIP (PAX transcription activation domain interacting protein), Q8N4P9; NBS1 (Nijmegen breakage syndrome protein 1, NIBRIN), O60934; Rev1 (DNA repair protein Rev1), P12689; Rap1 (DNA-binding protein Rap1, SBF-E), P11938; Rad9 (DNA repair protein Rad9), P14737; XRCC1 (DNA repair protein XRCC1), P18887; TdT (terminal deoxynucleotidyltransferase), P04053; DNL4 (DNA ligase IV), P49917; (human), Q9LL84 (*Arabidopsis thaliana*); DNL3a (DNA ligase III, isoform α), P49916; DNLj (bacterial DNA ligase), O31498; DNApoll (DNA polymerase λ), Q9UGP5; DNApol3e (DNA polymerase III, ϵ subunit), Q97L28. Other abbreviations: Xenop., *Xenopus laevis*; S.cerev., *Saccharomyces cerevisiae*; Arabidopsis, *Arabidopsis thaliana*; B.sub, *Bacillus subtilis*; Clostr., *Clostridium acetobutylicum*.

Rev1, Rap1, and Rad9, the BRCA1-associated RING-domain protein BARD1 (*3*), NBS1 (Nijmegen breakage syndrome protein 1, NIBRIN, cell-cycle regulatory protein P95), the transcriptional transactivator and cell-cycle checkpoint protein MDC1 (mediator of DNA-damage checkpoint protein 1, NFBD1/KIAA0170) (*4*−*6*), the PAX transcription-activation domain-interacting protein PTIP, DNA ligases IV and IIIα, DNA polymerase λ, and the terminal deoxynucleotidyltransferase TdT, to name but a few (Figure 1B; reviewed in ref *7*).

Proteins containing BRCT domains display a broad range of biological activities and functional diversity. They have been implicated in transcriptional regulation, DNA repair, cell-cycle progression, and cancer suppression (*1*, *2*, *8*), as shown for Rad9, XRCC1 (*9*), 53BP1 (*10*), TopBP1 (*11*−*13*), MDC1 (*4*−*6*), and BRCA1 (*14*−*16*). BRCA1 is involved in transcription-coupled DNA repair (*17*) and the upregulation of genes in the apoptotic pathway (*18*). The tandem BRCT repeats of BRCA1 [termed here $(BRCT)_2$] are involved in cell-cycle regulation (*19*), apoptosis (*20*), cancer suppression (*21*), chromatin remodeling (*22*), and regulation of transcription (*23*−*26*), thereby modifying the expression levels of genes involved in breast cancer development (*27*). $(BRCT)_2$ of BRCA1 is shown to regulate p53-dependent gene expression by stimulating the expression of the CDK inhibitor $p21^{WAF1/CIP1}$ and MDM2 (*28*, *29*). The carboxy-terminal domain BRCT-c, represents the minimal transactivation domain (*24*), which itself is sufficient for the transactivation of $p21^{WAF1/CIP1}$. C-terminal truncations of more than 8 residues result in structural destabilization of the $(BRCT)_2$ and loss of activity (*28*−*31*). The disease-associated missense mutation Tyr1853stop, which deletes the last 11 residues of BRCA1, confers a very high risk of breast and ovarian cancer (*32*). Similar results have been obtained for mouse BRCA1 (*21*). Notably, most cancer-associated mutations in *BRCA1* affect the function of $(BRCT)_2$ (*33*−*35*).

The importance of the BRCT repeats is emphasized by the identification of binding partners which are integral components of vital biochemical processes such as DNA repair, replication, recombination and ligation, cell-cycle regulation, and tumor suppression. $(BRCT)_2$ of BRCA1 interacts with the DNA repair-associated helicase BACH1 (*15*), the retinoblastoma suppressor (Rb)-associated protein RbAp46, histone deacetylases HDAC1 and HDAC2 (*36*), and CtIP, a transcriptional corepressor in the CtBP pathway (*37*, *38*). The interaction between CtIP and $(BRCT)_2$ is disrupted upon DNA damage and critical in mediating transcriptional regulation of p21 in response to DNA damage (*38*). Interestingly, the BRCT domains of BRCA1 and

XRCC1 are shown to bind to ends of double-stranded DNA, a structural feature of DNA strand breaks (*39*). In addition, BRCA1 is reported to interact with the universal tumor suppressor protein p53 with BRCT-c being sufficient for the interaction with the DNA-binding domain of p53 (*29*, *40*). Recent results demonstrate that the BRCT repeats of PTIP and BRCA1 bind specifically to peptides phosphorylated by kinases ATM (ataxia telangiectasia-mutated) and ATR (ataxia telangiectasia- and RAD3-related) in response to γ-irradiation (*41*). In addition, the BRCT repeats of MDC1, BARD1, and DNA ligase IV were found to bind preferentially to peptides containing phosphoserine (*42*). $(BRCT)_2$ of BRCA1 interacts *in vivo* with BACH1 (*15*). This interaction depends on the phosphorylation status of BACH1 and is required for the G_2-M checkpoint control (*43*). Disease-associated BRCA1 mutations P1749R and M1775R, and truncated BRCA1 variants lacking BRCT-c, abolish the capacity to bind phosphorylated BACH1 (*43*). Notably, the single BRCT domain of the serine protease Fcp1 and BRCT-6 of TopBP1 (DNA topoisomerase II binding protein) bind to phosphorylated RNA polymerase II and transcription factor E2F1, respectively (*43*).

Structural data are available for the BRCT domains of BRCA1 (*44*, *45*), 53BP1 (*45*, *46*), XRCC1 (*47*), DNA ligase III (*48*), and a NAD^+-dependent DNA ligase (*49*). However, the molecular structure of an isolated BRCT domain that is normally part of a tandem repeat has never been reported. Recent structural studies revealed the molecular interaction of the tandem BRCT repeats from BRCA1 with phosphorylated peptides containing the consensus sequence pSer-X-X-Phe, as found in BACH1 (*49*−*51*). However, the underlying signaling events leading to BRCA1 activation and tumor suppression in response to DNA damage remains largely unclear. Particularly, the transcriptional activation function of the BRCT repeats is little understood. Mutagenesis studies showed that some cancer-associated mutations in BRCT-n abolish the transcriptional activation function of the dual repeat even in the presence of intact BRCT-c (*23*, *24*, *30*). These findings suggest that BRCT-n may influence the activity of BRCT-c. The two BRCT domains are intimately connected, sharing a reasonably large and predominantly hydrophobic interface area (*44*). This led us to the hypothesis that the structural integrity of the interface is crucial for the biological activity of the BRCT tandem repeats. To explore this possibility and to gain further insight into BRCT domains in the solution state, we have determined the NMR structure of the isolated BRCT-c domain from human BRCA1 (residues 1755−1863) and further used NMR to study the dynamics of this domain and investigate binding to previously reported interaction partners. The association behavior of both BRCT-c and the tandem repeat $(BRCT)_2$ was analyzed by analytical ultracentrifugation and size exclusion chromatography to address the dimerization properties of the BRCT region. Together, these data may provide clues about the structure−function relationship of the individual BRCT subdomains within the tandem repeat of BRCA1.

METHODS

Recombinant Gene Expression and Protein Purification. The DNA sequence encoding BRCT-c (residues 1755−1863 of BRCA1) was amplified by standard PCR methods and inserted into the expression plasmid pGEX-4T-1 (Amersham Biosciences). BRCT-c was expressed as a glutathione *S*-transferase (GST) fusion protein in *Escherichia coli* BL21[pREP4-groESL/CodonPlusRIL] cells. Coexpression with chaperonins GroEL and GroES encoded on the plasmid pREP4-groESL (Roche) improved the solubility and stability of BRCT-c. Cells harboring the CodonPlus RIL plasmid (Stratagene) encoding $tRNA^{Arg}$, $tRNA^{Ile}$, and $tRNA^{Leu}$ were used to avoid the problem of reduced expression levels due to the presence of rare codons in the recombinant gene. Cells were grown at 32 °C in M9 minimal medium (*53*) containing 100 mg/L carbenicillin, 30 mg/L kanamycin, and 34 mg/L chloramphenicol and supplemented with 1.3% (w/v) D-glucose. Expression was induced by addition of 0.5 mM IPTG, and cells were grown for an additional 5−8 h at 25 °C before they were lysed with a French press (2 × 1000 bar). The GST−BRCT-c fusion protein was purified by affinity chromatography on a glutathione−Sepharose 4B column (Amersham Biosciences). The GST moiety was cleaved with thrombin (Roche) and separated by size exclusion chromatography on a Superdex 75 column (Amersham Biosciences) to yield the BRCT-c domain with an additional N-terminal glycine (110 residues). The integrity of the cleavage product was verified by N-terminal sequencing and mass spectrometry. BRCT-c was then purified to homogeneity on a MonoQ anion-exchange column (Amersham Biosciences). Samples for NMR spectroscopy were desalted on a FastDesalting column (Amersham Biosciences) and concentrated using Ultrafree concentrators (Millipore). All chromatography steps were performed at 4 °C. The purity of the samples was estimated from overloaded silver-stained SDS−PAGEs. Protein concentrations were determined by UV absorption spectra with an extinction coefficient ϵ of 22 190 L mol^{-1} cm^{-1} at a wavelength of 280 nm.

Uniformly ^{15}N-labeled and ^{13}C-, ^{15}N-labeled BRCT-c samples were prepared by growing *E. coli* BL21 cells in M9 minimal medium (*53*) containing 0.5 g/L $^{15}NH_4Cl$ as the sole nitrogen source and either 1.3% (w/v) [$^{12}C_6$]-D-glucose or 0.5% (w/v) [$^{13}C_6$]-D-glucose, respectively, as the sole carbon source. Labeled protein samples were purified as described above.

NMR Spectroscopy and Structure Calculation. All NMR experiments were performed at 296 K using Bruker DRX600 and DMX750 spectrometers in standard configuration, with triple-resonance probes equipped with self-shielded gradient coils. Two samples of BRCT-c at pH 6.8 in a buffer containing 10 mM KH_2PO_4, 10 mM K_2HPO_4, 5 mM KCl, and 10 mM fresh fully deuterated DTT were used. A 1.3 mM ^{15}N-labeled sample in H_2O (containing 7% D_2O for the lock) was used for three-dimensional (3D) HNHA, HNHB, ^{15}N-edited NOESY and TOCSY, and ^{15}N T_1 and ^{15}N T_2 relaxation and heteronuclear $^1H-^{15}N$ NOE experiments. Two-dimensional (2D) NOESY, TOCSY, and DQF-COSY spectra were acquired in both H_2O (with 7% D_2O) and 99.98% (v/v) D_2O. A 0.7 mM ^{13}C-, ^{15}N-labeled sample was used for 3D CBCA(CO)NNH, CBCANNH, HBHA(CO)NNH, and HBHANNH experiments for the backbone and side chain assignment (reviewed in ref *54*). 3D HCCH-TOCSY and ^{13}C-edited NOESY spectra were also acquired. NOESY and TOCSY spectra were acquired with mixing times of 80 ms. ^{15}N T_1 and T_2 relaxation times were extracted from two series of 11 2D $^1H-^{15}N$ correlated spectra with

Table 1: Restraints and Structural Statistics for the Final BRCA1 BRCT-c Ensemble

Restraints		
total no. of experimental restraints	1969	
total no. of NOE restraints	1828	
intraresidue ($i = j$)	441	
sequential ($\|i - j\| = 1$)	414	
medium-range ($2 \leq \|i - j\| \leq 4$)	226	
long-range ($\|i - j\| > 4$)	747	
no. of H-bond restraints	33	
total no. of dihedral angle restraints	108	
experimental (HNHA)	38	
predicted (TALOS)	70	
average nonintraresidue NOEs per residue	12.6	
no. of NOE violations >0.3 Å	0	
no. of dihedral angles >5°	0	
$\varphi-\psi$ Space (residues[a])		
most favored regions (%)	68.7	
additionally allowed regions (%)	23.5	
generously allowed regions (%)	5.5	
residues in disallowed regions (%)	2.2	
	$(SA)_{ensemble}$[b]	$\langle SA\rangle_{scm}$[c]
Final Energies		
E_{total} (kcal/mol)	63.69 ± 0.77	63.27
E_{bonds} (kcal/mol)	2.48 ± 0.11	2.34
E_{angles} (kcal/mol)	33.34 ± 0.49	33.87
$E_{impropers}$ (kcal/mol)	2.91 ± 0.21	3.28
E_{vdW} (kcal/mol)	21.52 ± 0.90	20.11
E_{NOE} (kcal/mol)	3.18 ± 0.39	3.54
rmsds[d]		
deviation from ideal values		
bonds (Å)	0.0012 ± 0.00003	0.0011
angles (deg)	0.2654 ± 0.0019	0.265
impropers (deg)	0.1441 ± 0.0051	0.149
backbone Cα atoms (Å)	0.322 ± 0.0518	
non-hydrogen atoms (Å)	3.517 ± 0.9545	

[a] Calculated with PROCHECK-NMR (*73*). [b] $(SA)_{ensemble}$ represents the average rms deviations for the ensemble of 15 structures. [c] $\langle SA\rangle_{scm}$ represents the statistics for the structure closest to the mean. [d] Evaluated using CNS (*58*). Residues 6−17, 24−45, 52−57, and 71−101 of BRCT-c included in the rmsd calculations.

relaxation delays of 12, 52, 102, 152, 202, 302, 402, 602, 902, 2002, and 5002 ms for T_1 and 6, 10, 18, 26, 34, 42, 82, 122, 162, 202, and 242 ms for T_2. Rates and errors were fitted as implemented in SPARKY (*55*). All spectra were acquired essentially as described previously (*56*).

Data were processed using the XWIN-NMR program (version 1.3) of Bruker BioSpin GmbH (Rheinstetten, Germany) and the AZARA program (version 2.1) of W. Boucher (unpublished). Carbon, nitrogen, and proton resonances were assigned by standard assignment procedures from CBCA(CO)NNH, CBCANNH, HBHA(CO)NNH, and HBHANNH spectra. Assignment was carried out on Silicon Graphics O2 workstations using the interactive program ANSIG 3.3 (*57*). Structures were calculated from the restraints listed in Table 1 using XPLOR (version 3.1) and CNS (version 1.0) (*58*). Calculations were performed using a standard simulated annealing protocol starting from random coordinates. Distance restraints were classified as strong (≤2.5 Å), medium (≤3.5 Å), weak (≤5.0 Å), and very weak (≤6.0 Å). Intraresidue NOE distance restraints were omitted. The 15 lowest-energy structures with no distance violations greater than 0.3 Å and no angle violations greater than 5° were accepted into the final ensemble. A total of 108 dihedral angle restraints were obtained from $^3J_{HNHA}$ values extracted from a series of 2D ^{1}H−^{15}N *J*-modulated COSY spectra and backbone chemical shifts using TALOS (*59*). In addition, 33 hydrogen bond restraints were identified from a 2D ^{15}N HSQC spectrum following exchange into D_2O. The NMR structure of BRCT-c was determined independently from the crystal structure of the BRCA1 BRCT repeat region as described in ref *44*.

Interaction Mapping with DNA and the DNA-Binding Domain of p53. To define the interaction sites with potential binding partners, we performed titration experiments with ^{15}N-labeled BRCT-c, the DNA-binding domain of human p53 (p53-D, residues 94−292) and different 5′-phosphorylated and unphosphorylated double-stranded DNA oligomers which were prepared by slow-cool annealing of the self-complementary DNA oligomers 5′-pGCCTAGCTAGGC-3′, 5′-GCCTAGCTAGGC-3′, and 5′-GCGTACGC-3′. The binding partners were added to 0.2 mM BRCT-c up to a molar excess of 1.2:1.0. A series of 2D ^{1}H-^{15}N HSQC spectra were acquired and analyzed with respect to chemical shift perturbations (CSPs) upon addition of the binding partner. The pH was measured at every titration step to exclude CSPs caused by pH changes and different protonation states of histidine side chains.

Analytical Ultracentrifugation. Both sedimentation velocity (SV) and sedimentation equilibrium (SE) experiments were performed with a Beckman XL-I analytical ultracentrifuge (Beckman-Coulter, Fullerton, CA) in a four-hole AN Ti60 rotor using the ^{15}N-labeled protein. The partial specific volume ($\bar{\nu}$) of BRCT-c was calculated from the sequence (*60*, *61*) and corrected to account for complete labeling with ^{15}N by considering the mass ratio of unlabeled over ^{15}N-labeled protein:

$$\bar{\nu}_{^{15}\mathrm{N-labeled}} = \bar{\nu}_{\mathrm{unlabeled}}(\mathrm{MW}_{\mathrm{unlabeled}}/\mathrm{MW}_{^{15}\mathrm{N-labeled}})$$

All samples were analyzed in a buffer containing 10 mM KH_2PO_4, 10 mM K_2HPO_4, 50 mM KCl, and 5 mM DTT (pH 6.8). The density of the buffer used was measured with a DMA 58 densitometer (Anton Paar, Graz, Austria). An aliquot of buffer in dialysis equilibrium with the protein solution was used as a reference in all concentration measurements. SV experiments were performed at 20 °C and 50 000 rpm in double-sector charcoal-filled Epon centerpieces with a path length of 12 mm. Scans were recorded at a single wavelength (295 nm) every 90 s with a Δr (radial step size) of 0.003 cm with an initial loading concentration of 0.6, 0.8, or 1.0 mg/mL (0.05, 0.06 or 0.08 mM). Data were analyzed by direct fitting to the Lamm equation (*62*−*65*) and by the method of van Holde-Weischet (*66*, *67*).

SE experiments were performed at 4 °C and 30 000 rpm in six-sector charcoal-filled Epon centerpieces with loading concentrations ranging from 0.4 to 1.2 mg/mL (from 0.03 to 0.10 mM) with 0.1 mg/mL increments for the nine available sectors. Scans were recorded with a Δr of 0.001 cm and 30 replicate measurements at every step point, at three different wavelengths for each sector. The extinction coefficient of BRCT-c at the required wavelength was calculated from a UV spectrum, using a theoretical extinction coefficient as a reference (*68*).

After equilibrium had been reached, data were fitted to a single-ideal species model of the form

$$c_r = c_0 e^{MF} + \delta \quad (1)$$

with

$$F = \frac{(1 - \rho v)\omega^2(r^2 - r_0^2)}{2RT} \quad (2)$$

using the general nonlinear least-squares procedures as described previously (*69*) and the extensions of eq 1 for multiple species in reversibly associating equilibrium (*70*), taking into account the association constants. The statistical relevance of the different parameter estimates was tested via Monte Carlo simulations using 20 000 iterations for each model. Data were analyzed using LAMM (*65*), SedFit 8.3 (*63*), and UltraScan5.0 (Demeler, University of Texas Health Sciences Center, San Antonio, TX).

Size Exclusion Chromatography. To investigate the dimerization behavior of both the isolated BRCT-c domain and the tandem repeat $(BRCT)_2$ (residues 1646−1863 of BRCA1), size exclusion chromatography was carried out using the HiLoad Superdex 75 (26/60) column (Amersham Biosciences). Several runs were performed at a flow rate of 2.5 mL/min with phosphate buffer in the pH range of 6.8−8.0, 60−150 mM KCl, and 5 mM DTT. The apparent molecular mass was determined by comparing the elution volume with the values for BSA (67 kDa), ovalbumin (44 kDa), chymotrypsinogen A (25 kDa), and myoglobulin (17 kDa) used for calibration.

RESULTS

Solution NMR Structure of the BRCT-c Domain from Human BRCA1. The structure of BRCT-c was determined using triple-resonance, multidimensional NMR spectroscopy on 1.3 mM ^{15}N-labeled and 0.7 mM ^{13}C-, ^{15}N-labeled protein samples. The final ensemble of structures was calculated from the restraints listed in Table 1.

BRCT-c is defined well by an average of 12.6 inter-residue NOE distance restraints per residue. The ensemble consisting of the 15 lowest-energy structures has a mean backbone rms deviation (rmsd) of 0.311 Å for the well-structured regions (residues 1759−1770, 1777−1798, 1805−1810, and 1824−1854 of BRCA1, corresponding to positions 6−17*, 24−45*, 52−57*, and 71−101*, respectively, in our BRCT-c construct). The backbone rmsd over the residues 1759−1854 (6−101*) is 0.696 Å. BRCT-c consists of four parallel β-strands surrounded by three α-helices with β1α1β2β3α2β4α3 topology (Figure 2). The β-sheet displays a left-handed β-twist (known from other β-proteins) and is stabilized mostly by hydrophobic interactions involving residues Ile1766−Cys1768 (I13−C15*) of β1 and Ile1807−Val1810 (I54−V57*) of β3. Strands β2 and β4 form the outside of the β-sheet. Helix α2 comprises residues Ile1824−Met1827 (I71−M74*) and is located at the end of loop 3 [residues 1812−1823 (59−70*)]. The signals in the ^{15}N-edited NOESY spectra from residues in loop 3 were consistently weak, indicating that magnetization in these regions is rapidly lost by relaxation or exchange processes. Consequently, this region of the molecule is very poorly restrained in the NMR structure. Similarly, loop 1 [residues 1773−1777 (20−24*)], which connects β1 and α1, and loop 2 [residues 1799−1804 (46−51*)], which precedes β3, have few experimental restraints and display more conformational variation in the ensemble (Figure 2A). No inter-residue NOEs could be assigned for the N-terminal glycine residues 1755 (2*), 1774 (21*), 1819 (66*), and the C-terminal residues 1860−1863 (107−110*). The rotational correlation time (τ_c) was 9.9 ns.

Dynamics of BRCT-c from NMR Measurements. To assess the degree of internal mobility of BRCT-c, we performed ^{15}N T_1 and T_2 relaxation and ^{1}H−^{15}N heteronuclear NOE experiments (Figure 3). These data showed that residues 1755−1758 (1−5*) at the N-terminus and residues 1856−1863 (103−110*) at the C-terminus were flexible. In addition, the relaxation data show elevated ^{15}N T_1 and T_2 values and more negative ^{15}N−^{1}H heteronuclear NOEs for residues in loops 1−3, indicating internal mobility of these regions. The loops are characterized by only very few medium- and long-range NOEs (Figure 4A) and higher-than-average rmsd values for the Cα atoms in the corresponding NMR structures (Figure 4B). This is in agreement with the crystal structure (*44*) which showed these loop regions to have increased *B*-factors (Figure 4C). In loop 3, most side chains were poorly defined by the electron density map and no model was built for residues 1817−1819 (64−66*), indicating a high degree of disorder and increased mobility of these residues in the crystal. Superposition of the NMR ensemble onto the crystal structure of BRCT-c is shown in Figure 2C.

Conserved Residues and Cancer-Associated Mutations. Most of the conserved residues in BRCT domains are located in the central β-sheet where they mediate important hydrophobic interactions. In BRCT-c, these are Leu1764 (L11*), Ile1766 (I13*), Cys1767 (C14*), and Cys1768 (C15*) in β1, Val1791 (V38*) in β2, Ile1807 (I54*), Val1808 (V55*), Val1809 (V56*), and Val1810 (V57*) in β3, and Val1832 (V79*) and Val1833 (V80*) in β4. Additional conserved residues are found in helices α1 and α3 (Figure 1B). α1 is anchored to the core through Val1784 (V31*) which contacts Val1791 (V38*) from β2 and Ile1766 (I13*) from β1. Leu1780 (L27*) interacts with Cys1768 (C15*) from β1 and Val1838 (V85*) from α3. Met1783 (M30*) from α1 contacts Val1842 (V89*) from α3. Helix α3 harbors the most conserved residue within the BRCT family, Trp1837 (W84*), which is deeply buried within the hydrophobic core and crucial for the stabilization of the BRCT fold. The stability of $(BRCT)_2$ is greatly reduced by the missense mutations Trp1837Arg (W84R*) and Trp1837Gly (W84G*) (*31*). Trp1837 (W84*) makes direct contact with Leu1764 (L11*) and Ile1766 (I13*) from β1, Val1808 (V55*) and Val1810 (V57*) from β3, and Val1833 (V80*) from β4 as well as Val1784 (V31*) from α1. In addition, Trp1837 (W84*) interacts with Leu1850 (L97*) and two highly conserved aromatic residues, Phe1761 (F8*) and Tyr1853 (Y100*), at either end of the BRCT-c sequence (Figures 1B and 2A). Phe1761 (F8*) makes additional contacts with Leu1764 (L11*) and Ile1766 (I13*) from β1, with Val1784 (V31*) from α1, and with Val1838 (V85*) from α3 and also with Cys1787 (C34*), Ala1789 (A36*), and Cys1847 (C94*). Although in the immediate vicinity of Trp1837 (W84*), Tyr1853 (Y100*) is only partially embedded in the hydrophobic core. Other important core interactions are with Val1833 (V80*) from β4 and Leu1850 (L97*) located in the turn at the end of helix α3. Several conserved Gly and Ala residues at specific positions are particularly important. One of the most conserved residues in BRCT domains is Gly1788 (G35*) which is located in the turn connecting α1

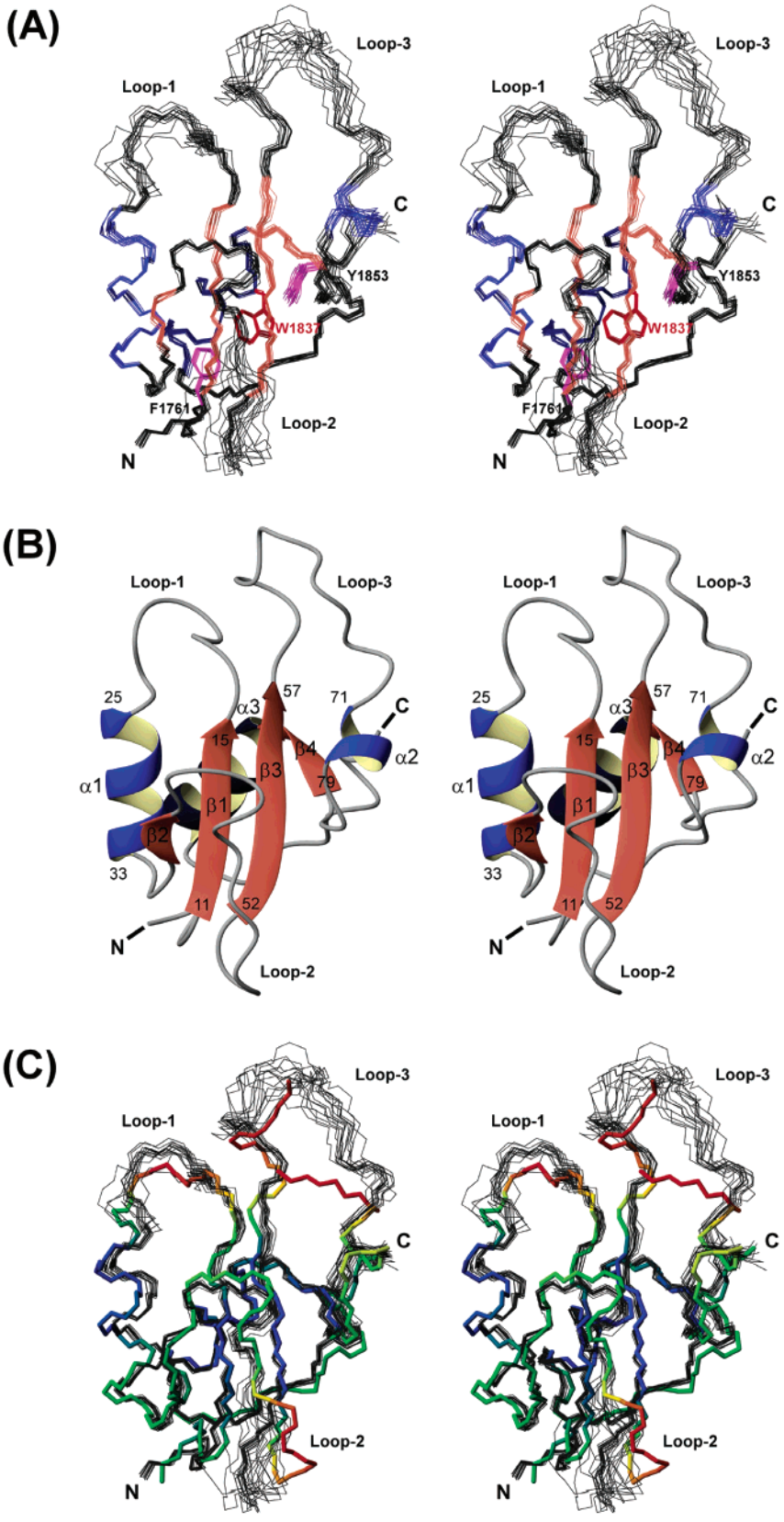

FIGURE 2: Solution NMR structure of BRCT-c. (A) Superposition of the backbone (N, Cα, and C′) atoms for the 15 lowest-energy structures of the BRCA1 BRCT-c domain, residues 1759−1855 (6−102*) (stereoview). β-Strands (β1−β4) and α-helices (α1−α3) are colored light brown and blue, respectively. Loop regions are labeled as Loop-1, Loop-2, and Loop-3. The three most conserved aromatic core residues, Phe1761 (F8*), Tyr1853 (Y100*), and Trp1837 (W84*), are shown in magenta and red, respectively. The structural statistics are given in Table 1. (B) Ribbon diagram of the BRCT-c structure closest to the mean (scm). The hydrophobic core is formed by the central β-sheet with highly conserved aromatic residues. (C) Superposition of the NMR ensemble (backbone atoms of the 15 lowest-energy structures) and the crystal structure of BRCT-c (*44*). The latter is colored according to the crystallographic *B* values: blue (≤30 Å^2), green (∼40 Å^2), yellow (∼50 Å^2), and red (≥60 Å^2). Figures were created using MolMol (*74*).

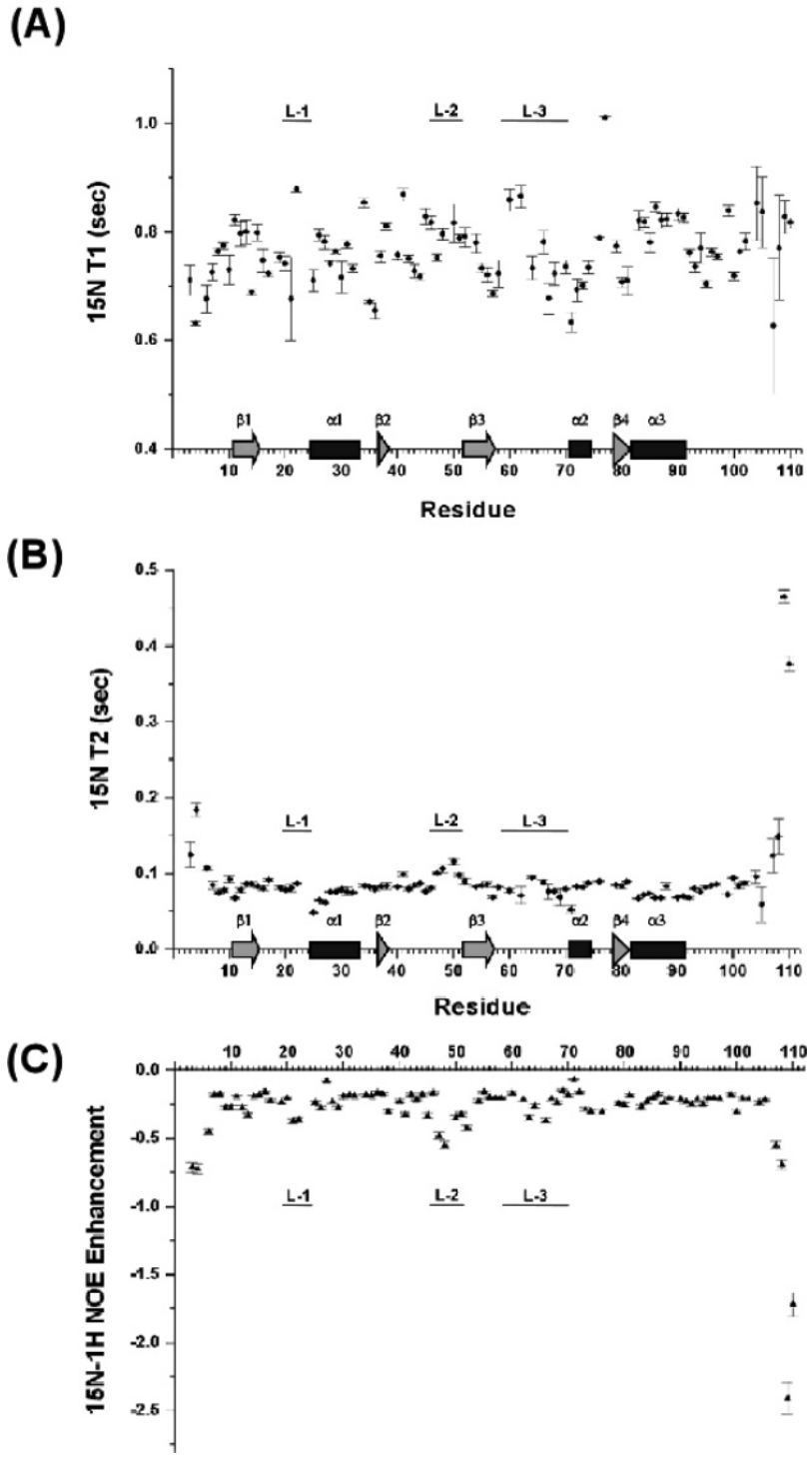

FIGURE 3: Dynamics from NMR data. (A) ^{15}N T_1 relaxation data. (B) ^{15}N T_2 relaxation data. (C) ^{1}H−^{15}N heteronuclear NOE data. Slowly relaxing, flexible loop regions are marked with L-1−L-3. β-Strands and α-helices are indicated schematically.

and β2 (Figure 1B). The structure of BRCT-c reveals that only Gly fits into the limited space available in this area. This applies also to the subsequent position, Ala1789 (A36*), and to a lesser extent to Gly1763 (G10*) and Gly1770 (G17*). Substitution of these small residues with larger side chains would be likely to result in destabilization or misfolding. Consistently, the mutation Gly1788Val (G35V*) renders $(BRCT)_2$ highly sensitive to proteolytic degradation (*31*). Additional missense mutations are Ile1766Ser (I13S*), Met1783Thr (M30T*), Val1804Asp (V51D*), Val1809Phe (V56F*), and Tyr1853Cys (Y100C*). Most of these substitutions destabilize the BRCT fold by interfering with BRCT substructures or altering the BRCT-n−BRCT-c interface (*31*) and are therefore very likely to be functionally deleterious.

The solution structure of BRCT-c overlays well with the crystal structure of the second domain from the BRCT tandem repeat of BRCA1 (*44*) but shows subtle differences at the BRCT-n−BRCT-c interface and in three flexible loop regions (Figure 2C). The overall backbone rmsd is 0.967 Å for the well-structured regions, residues 1759−1770 (6−17*), 1777−1798 (24−45*), 1805−1810 (52−57*), and 1824−1854 (71−101*). The interface of the tandem BRCT repeats is predominantly hydrophobic and involves residues from helices α1, α2-n (helix α2 in BRCT-n), and, to a lesser

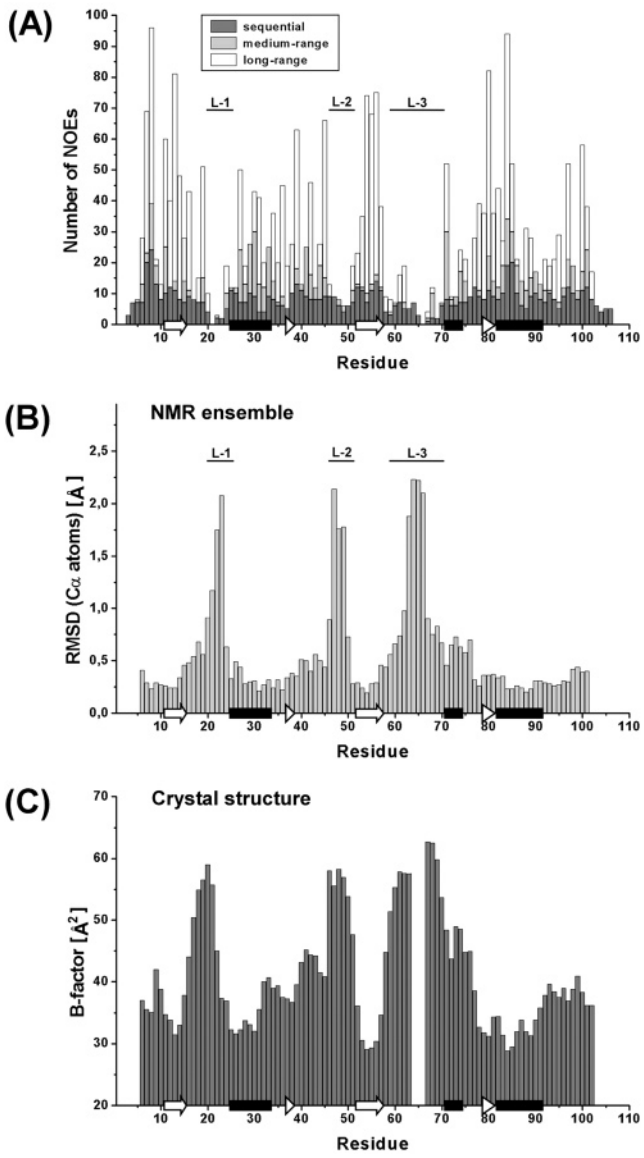

FIGURE 4: Precision of the BRCT-c structure. (A) Number of sequential, medium-range, and long-range NOE distance restraints per residue. β-Strands and α-helices are indicated schematically. Loop regions are marked with L-1−L-3. (B) rmsd values of Cα atoms for residues 6−101* of BRCT-c (residues 1759−1854 in BRCA1). The 15 lowest-energy structures are considered. (C) *B* factors for Cα atoms of residues 1759−1854 of BRCA1 as determined by X-ray crystallography at 2.5 Å resolution (*44*). Residues 1817−1819 (residues 64−66* of BRCT-c) are missing in the crystal structure.

extent, α3. In the absence of BRCT-n, residues of BRCT-c located at the interface become solvent-exposed and undergo conformational changes. This affects the orientation of α1 and α3 with respect to each other. The changes in this region of BRCT-c can be attributed to the absence of the intramolecular tandem partner BRCT-n in our NMR study. Most striking is the reorientation of Met1775 (M22*) near the end of loop 1, which is correlated with the tumor suppressor function of BRCA1. In the presence of BRCT-n, the side chain of Met1775 (M22*) extends into the BRCT-n−BRCT-c interface and contributes to the Phe(+3) binding pocket (*50*−*52*), the second major binding epitope for phosphoserine containing BACH1 peptides, thereby forming a hydrophobic contact with Met1783 (M30*) (α1), Leu1839 (L86*) (α3), and Leu1701 (α2-n), whereas in the isolated BRCT-c domain, Met1775 (M22*) loses contact with all other interface residues and becomes solvent-exposed by moving its side chain to the opposite direction. The NMR relaxation data, especially the values for T_2 and $^1H-^{15}N$ heteronuclear NOE enhancement (Figure 3), point at an increased internal flexibility of this residue in solution. This is reflected in the fact that no long-range NOEs could be assigned for Met1775 (M22*) and the rmsd value of its Cα atom with respect to the mean position in the ensemble is substantially increased (Figure 4). The structure of $(BRCT)_2$ harboring the cancer-predisposing mutation Met1775Arg (M22R*) is similar to the wild type but shows rearrangement of the BRCT-n−BRCT-c interface and destabilization of the domain (*71*). As shown by our NMR study, the structural effects are even more pronounced in the case of the complete absence of BRCT-n. This indicates that BRCT-n may cause BRCT-c to adopt a biologically active conformation by forming a compact BRCT-n−BRCT-c interface.

Analysis of the hydrophobic surface potential of BRCT-c revealed two solvent-accessible, hydrophobic channels bounded by more flexible sections of the molecule. One region involves the exposed side chains of Tyr1769 (Y16*), Met1827 (M74*), and partially Trp1815 (W62*) which reside in a cleft lined by charged residues Glu1794 (E41*) and Glu1817 (E64*) from loop 2 and loop 3, respectively (Figure 5A,C). The second area is located opposite the BRCT-n−BRCT-c interface (Figure 5B,D). It is characterized by mostly hydrophobic residues from β1, β3, β4, and the region C-terminal to α3, including Leu1764 (L11*), Ile1807 (I54*), Pro1812 (P59*), Phe1821 (F68*), Pro1831 (P78*), Cys1847 (C94*), and Leu1850 (L97*). This array is flanked by Leu1800 (L47*) from loop 2, His1805 (H52*) and His1822 (H69*) from β3 and loop 3, respectively, and Glu1849 (E96*). Interestingly, Ile1807 (I54*) in BRCA1 BRCT-c is replaced with a conserved His in many other BRCT domains (Figure 1B) and thereby occupies a position in space adjacent to His1805 (H52*) on β3. These two solvent-exposed, hydrophobic regions appear to be good candidates for putative interfaces with BRCT-c binding partners.

Interaction Mapping with DNA and the DNA-Binding Domain of p53. A series of $^{15}N-^1H$ chemical shift titration experiments were performed with DNA oligomers and p53-D as potential binding partners. Chemical shift perturbations (CSPs) were monitored by 2D ^{15}N-edited HSQC spectra as described in Methods. Previous studies reported a physical interaction between BRCT-c and the DNA-binding domain of p53 as determined from GST pull down assays (*29*). Despite these reports, we did not detect a direct molecular interaction between BRCT-c and p53-D. This result correlates with more recent work which show the molecular interaction between p53-D and the BRCT repeats of 53BP1 to be mediated exclusively by the N-terminal domain BRCT-n and the inter-repeat linker (*45*, *46*). In addition, BRCT-c did not exhibit CSPs in the presence of the DNA oligomers that were investigated, although BRCT-c is reported to be sufficient for DNA binding, albeit with reduced activity compared to that of $(BRCT)_2$ (*39*).

Association Behavior of BRCT-c: Analytical Ultracentrifugation Experiments and Size Exclusion Chromatography. The crystal structure of the second BRCT domain of XRCC1 shows a BRCT homodimer in the asymmetric unit (*47*). This

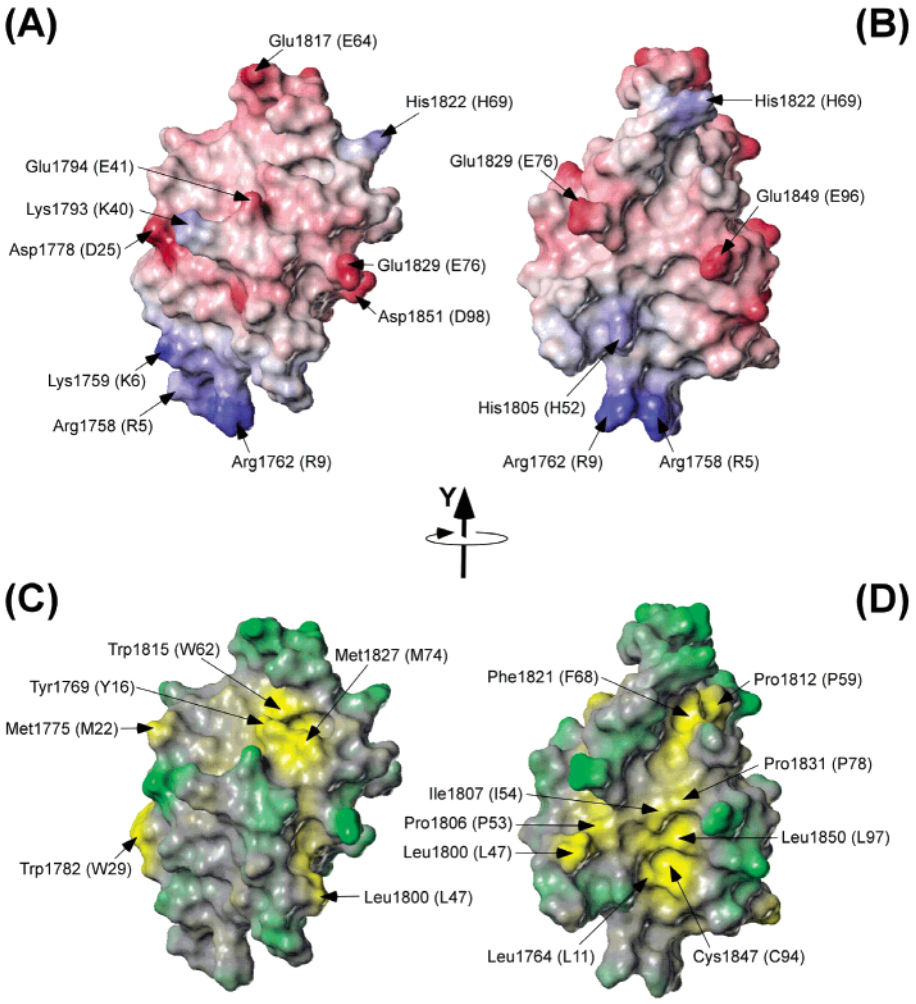

FIGURE 5: Surface potentials of BRCT-c. (A) Electrostatic potential of the solvent-accessible surface of BRCT-c [residues 1758−1856 (5−103*) shown]. Negative potential is shown in red and positive potential in blue. The orientation of the molecules is as in Figure 2. (B) Electrostatic potential with BRCT-c rotated around the *Y* and *Z* axes. (C) Hydrophobic (yellow) and hydrophilic (green) regions of BRCT-c. The orientation is the same as that in panel A. (D) Hydrophobic (yellow) and hydrophilic (green) regions. The orientation is the same as that in panel C. Figures were created using SYBYL (version 6.9.1, Tripos Inc., 2003).

suggested that BRCT domains in general might form homodimers or heterodimers with homologous BRCT domains. To investigate the self-association behavior of BRCA1 BRCT-c, we performed analytical ultracentrifugation experiments. Experiments were carried out in 50 mM KCl and 5 mM DTT at pH 6.8 and 20 °C.

As a first diagnostic of mass-driven self-association, we performed SV experiments at different concentrations to reveal concentration-dependent heterogeneity in the sedimentation behavior of BRCT-c. A cumulative van Holde-Weischet plot of the boundaries indicated only weak association. Direct fitting of the sedimentograms to the Lamm equation yielded apparent molecular masses close to the theoretical molecular mass for the ^{15}N-labeled monomeric BRCT-c domain (12.5 kDa), thus indicating very little multimerization. To obtain absolute values for the apparent molecular mass in solution, we performed a global fit on equilibrium gradients to eq 1, which converged to a molecular mass of 16.5 ± 0.1 kDa. This result excluded the possibilities of either a pure dimer or a pure monomer. Deconvoluting the data using a monomer−dimer self-association model resulted in a molecular mass for the monomeric species of 12.2 ± 0.8 kDa, which is in very good agreement with the theoretical value of 12.5 kDa (Figure 6). The dissociation constant (K_d) of 3.7 (+6.3/−2.2) mM as derived from ln K_d (8.2 ± 0.5 M) from the plot in Figure 6B suggests a fairly weak self-association of BRCT-c in solution. This is consistent with the observation that BRCT-c shows a tendency toward (unspecific) self-association in high-salt solutions at protein concentrations in the millimolar range. Monte Carlo distributions of the estimated parameter values for the apparent molecular mass and the dissociation constant are shown in Figure 6B, together with best fits to a Gaussian distribution, from which the standard deviations were obtained. In addition to analytical ultracentrifugation, we used size exclusion chromatography to investigate the association behavior of (i) the isolated BRCT-c domain and (ii) the tandem repeat $(BRCT)_2$ (25.2 kDa). In agreement with our ultracentrifugation results, both BRCT-c and the double repeat $(BRCT)_2$ eluted as monomers with apparent molecular masses of 10.3 and 24.3 kDa, respectively.

DISCUSSION

A comparison of the different BRCT structures determined to date shows that all these domains possess a common fold consisting of a central four-stranded parallel β-sheet flanked by three α-helices. Helices α1 and α3 are more conserved in sequence and length and provide intramolecular interaction

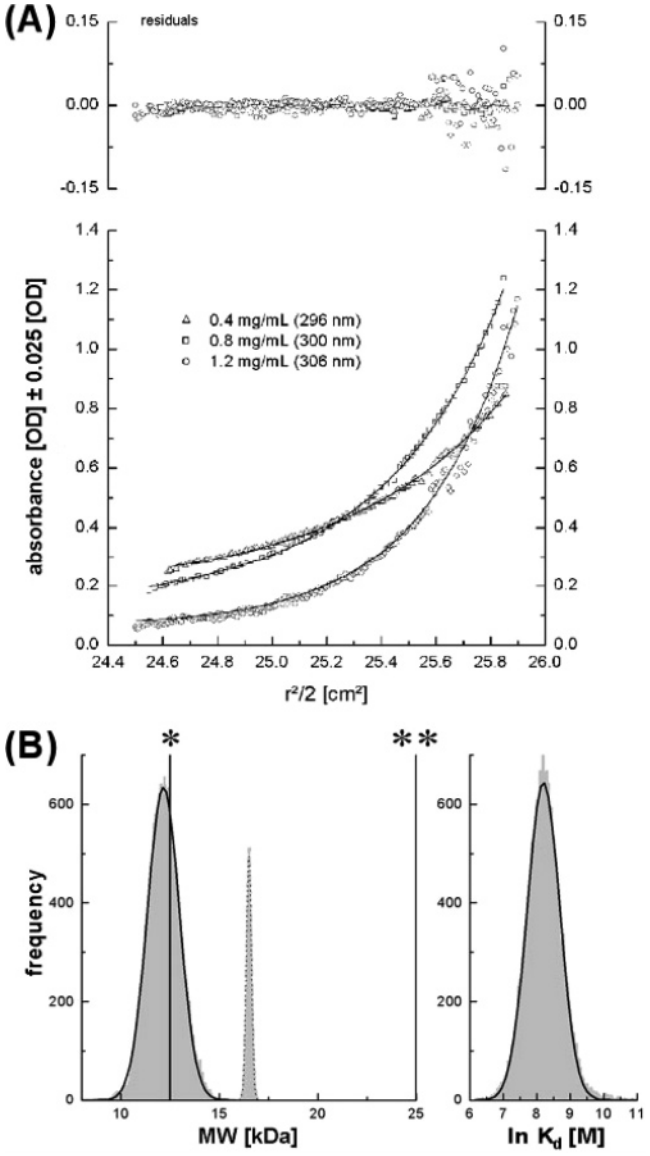

FIGURE 6: Analytical ultracentrifugation. (A) Global fit of the equilibrium gradients obtained with 0.4, 0.8, and 1.2 mg/mL (0.03, 0.06, and 0.1 mM, respectively) loading concentrations to the monomer−dimer model. Solid lines represent the best fits. Corresponding residuals are shown at the top. (B) Monte Carlo distributions (gray) of the molecular mass parameter and the dissociation constant parameter together with the best fit to a Gaussian distribution of the data (solid line for the monomer−dimer model; dotted line for the single-ideal species model). One asterisk and two asterisks indicate the theoretical molecular mass of the monomer and dimer, respectively.

sites to BRCT-n domains within tandem BRCT arrays. Loop 3 and helix α2 are the most variable sequence regions. In the tandem repeat, α2 of BRCT-n (α2-n) interacts with α1 and α3 of BRCT-c to form the BRCT-n−BRCT-c interface, whereas in BRCT-c, α2 has no such interaction with α1 and α3 from an adjacent BRCT domain. α2 can be as short as one turn, as in BRCT-c of BRCA1, or extended to three helical turns as seen in the second BRCT domain from XRCC1 (*47*). Loop 1 (which connects β1 with α1) and loop 2 (preceding β3) both allow sequence insertions with striking differences in length (Figure 1B).

A small number of key residues appear to be essential for the stabilization of the BRCT fold. These include the highly conserved aromatic core residues Trp1837 (W84*), Phe1761 (F8*), and Tyr1853 (Y100*), aliphatic residues Leu1780 (L27*) and Val1784 (V31*) which anchor α1 to the central β-sheet, Val1838 (V85*) and Val1842 (V89*) from α3 which contact α1 through hydrophobic interactions with Leu1780 (L27*) and Met1783 (M30*), respectively, and a number of additional hydrophobic residues mostly from the extended central β-strands β1 and β3. BRCA1 variants with mutations in these conserved regions of BRCT-c are correlated with an increased risk for the development of breast and ovarian cancer, highlighting the importance of an intact BRCT-c domain for the biological function of BRCA1. One of the most striking cancer-predisposing mutations in BRCA1 is the nonsense mutation Tyr1853stop (Y100X*) which truncates the protein by 11 residues and renders the BRCT tandem repeat sensitive to proteolytic degradation (*31*, *44*). This may point to an important role in stabilization by means of hydrophobic interactions which is supported by the fact that Tyr1853 (Y100*) contacts the central invariant Trp1837 (W84*). For a substantial number of BRCA1 mutations, the link to cancer is unclear because of a lack of distinctive segregation analysis data for affected families of patients (*35*). Using a combination of mutagenesis data and the three-dimensional structure of isolated BRCT-c and the tandem repeats, it may be possible to improve the assessment of cancer risks associated with previously uncharacterized mutations. The use of NMR as a method provides resonance assignments which may be monitored in chemical shift mapping experiments to identify new interaction partners and the specific residues involved in binding them.

The self-association behavior of BRCT-c, analyzed by means of analytical ultracentrifugation experiments, showed BRCT-c to be essentially monomeric with only a minor fraction of dimer. The results exclude the possibility that BRCT-c forms permanent homodimers in solution under near-physiological conditions. The observed slight tendency of BRCT-c to form dimers could be due to the interaction of solvent-exposed hydrophobic residues from α1 and α3, which are located at the BRCT-n−BRCT-c interface in the complete BRCT tandem repeat (*44*). This is also reflected in the molecular correlation time ($\tau_c = 9.9$ ns) measured by NMR, which is somewhat higher than values normally expected for proteins of this size (12.5 kDa).

Dynamics of BRCT-c from NMR and Biological Implications. The most prominent differences between the various BRCT domains are the lengths of loop 1, loop 2, and the region comprising loop 3 and helix α2 (Figure 1B). ^{15}N relaxation experiments showed the loop regions to be genuinely flexible in solution. This is also reflected by the small number of medium- and long-range NOEs observed for these residues (Figure 4A) and the higher rmsd values of their Cα atoms from the mean structure of the ensemble (Figure 4B). Interestingly, the crystal packing of $(BRCT)_2$ showed that loop 3 and α2 of BRCT-c interact with α1 and α3 of BRCT-n from neighboring BRCT repeats in a head-to-tail orientation (*44*). This intermolecular interaction of α-helices resembles the intramolecular interaction between BRCT-n and BRCT-c mediated by α2-n from BRCT-n and α1 and α3 from BRCT-c and might point to a more general interaction mode of multiple BRCT domains.

Further variations between different BRCT domains are observed in their surface potentials. Notably, the BRCT domains differ with respect to the electrostatic and hydro-

phobic surface properties in two solvent-accessible channels which could provide binding sites for target effector molecules (Figure 5). These differences may account for the broad range of biological functions associated with BRCT domains. This is supported by the existence of shortened BRCT variants, as found in the BRCA1-binding protein BARD1 and some DNA-modifying enzymes such as eukaryotic DNA ligase IIIα, bacterial DNA ligase, and the DNA polymerase IIIϵ from *Clostridium acetobutylicum* (Figure 1B), which lack the C-terminal hydrophobic cluster consisting of Tyr1853 (Y100*), Leu1854 (L101*), and Ile1855 (I102*) present in BRCA1. In contrast, the BRCA1 variant Tyr1853stop (Y100X*) confers a very high risk for breast and ovarian cancer, underlining the particular importance of this residue for the biological activity of BRCA1.

In BRCA1, BRCT-n and BRCT-c are intimately connected with each other by mostly hydrophobic interactions, and the tandem repeat $(BRCT)_2$ displays a very strong resistance to proteolytic degradation (ref *44* and unpublished data). It can therefore be considered a single structural unit as opposed to two individual domains. Nevertheless, the isolated BRCT-c domain is well-structured in solution. The NMR solution structure demonstrates that BRCT-c is capable of folding independently in the absence of its homologous intramolecular counterpart BRCT-n. Such an ability to fold independently either in the presence or in the absence of a complementary BRCT domain makes the BRCT domain a versatile building block for multidomain proteins and protein complexes with diverse biological function.

The NMR study presented here shows the first reported structure of an isolated BRCT domain from a tandem repeat. Comparison with the crystal structure of $(BRCT)_2$ reveals subtle conformational changes of BRCT-c in the absence of its intramolecular counterpart BRCT-n. These changes are characterized by the reorientation of helices α1 and α3 and affect the BRCT-n−BRCT-c interface and sites involved in the binding to phosphorylated peptides. Although not substantial, the conformational changes of BRCT-c in the absence of BRCT-n result in reduced activity of BRCT-c as determined by transcriptional activation assays. Interestingly, several mutations in BRCT-n, some of them located in helix α2-n which contributes to the BRCT-n−BRCT-c interface, are known to abolish this activity completely even in the presence of an intact BRCT-c domain (*23*, *24*, *30*). These findings indicate that the structural integrity and native conformation of BRCT-c are necessary but not sufficient for the biological function of the tandem repeats. In addition to the presence of an intact BRCT-c domain, BRCT-n and a properly aligned BRCT-n−BRCT-c interface appear to be essential for the tumor suppressor function of BRCA1. This view is strongly supported by recent structural studies showing that the interface region of the tandem BRCT repeats from BRCA1 is involved in recognition and binding of phosphorylated peptides containing the consensus motif pSer-X-X-Phe (*50*−*52*). We therefore conclude that one function of BRCT-n may be to guide BRCT-c into a biologically active conformation through the mostly hydrophobic interactions at the BRCT-n−BRCT-c interface. The combination of two or more BRCT domains within a single polypeptide chain then allows for subtle structural changes which may have a substantial impact on the biological function and activity. This could provide new insights into the structural and functional properties associated with dual or multiple BRCT repeats.

BRCT domains have been shown to be important players in numerous multicomponent networks, thereby implicating them in a substantial number of different cellular functions (*72*). The emerging picture is that BRCT domains have evolved with the capacity to perform a broad range of biological functions, with only a small number of conserved residues being essential for the formation and stabilization of the BRCT fold. The variable regions of BRCT sequences account for the functional diversity associated with BRCT domains from different families of proteins, and allow a precise fine-tuning of structure and function. Consistent with this high diversity, no BRCT domain has been shown to be capable of rescuing the function of a homologous BRCT domain *in vivo*.

ACKNOWLEDGMENT

We thank Drs. Albrecht Otto and Eva-Christina Müller for protein sequencing and mass spectrometry.

SUPPORTING INFORMATION AVAILABLE

Assigned $^{1}H-^{15}N$ HSQC spectrum of BRCT-c from human BRCA1 (residues 1755−1863) recorded at 296 K on a Bruker DMX 750 spectrometer. This material is available free of charge via the Internet at http://pubs.acs.org.

REFERENCES

1. Bork, P., Hofmann, K., Bucher, P., Neuwald, A. F., Altschul, S. F., and Koonin, E. V. (1997) A superfamily of conserved domains in DNA damage-responsive cell cycle checkpoint proteins, *FASEB J. 11*, 68−76.
2. Callebaut, I., and Mornon, J. P. (1997) From BRCA1 to RAP1: a widespread BRCT module closely associated with DNA repair, *FEBS Lett. 400*, 25−30.
3. Wu, L. C., Wang, Z. W., Tsan, J. T., Spillman, M. A., Phung, A., Xu, X. L., Yang, M. C., Hwang, L. Y., Bowcock, A. M., and Baer, R. (1996) Identification of a RING protein that can interact in vivo with the BRCA1 gene product, *Nat. Genet. 14*, 430−440.
4. Goldberg, M., Stucki, M., Falck, J., D'Amours, D., Rahman, D., Pappin, D., Bartek, J., and Jackson, S. P. (2003) MDC1 is required for the intra-S-phase DNA damage checkpoint, *Nature 421*, 952−956.
5. Lou, Z., Minter-Dykhouse, K., Wu, X., and Chen, J. (2003) MDC1 is coupled to activate CHK2 in mammalian DNA damage response pathways, *Nature 421*, 957−961.
6. Stewart, G. S., Wang, B., Bignell, C. R., Taylor, A. M., and Elledge, S. J. (2003) MDC1 is a mediator of the mammalian DNA damage checkpoint, *Nature 421*, 961−966.
7. Caldecott, K. W. (2003) Cell signaling. The BRCT domain: signaling with friends? *Science 302*, 579−580.
8. Koonin, E. V., Altschul, S. F., and Bork, P. (1996) BRCA1 protein products ... functional motifs ..., *Nat. Genet. 13*, 266−268.
9. Moore, D. J., Taylor, R. M., Clements, P., and Caldecott, K. W. (2000) Mutation of a BRCT domain selectively disrupts DNA single-strand break repair in non-cycling Chinese hamster ovary cells, *Proc. Natl. Acad. Sci. U.S.A. 97*, 13649−13654.
10. Xia, Z., Morales, J. C., Dunphy, W. G., and Carpenter, P. B. (2001) Negative cell cycle regulation and DNA damage-inducible phosphorylation of the BRCT protein 53BP1, *J. Biol. Chem. 276*, 2708−2718.
11. Makiniemi, M., Hillukkala, T., Tuusa, J., Reini, K., Vaara, M., Huang, D., Pospiech, H., Majuri, I., Westerling, T., Makela, T. P., and Syvaoja, J. E. (2001) BRCT domain-containing protein TopBP1 functions in DNA replication and damage response, *J. Biol. Chem. 276*, 30399−30406.
12. Yamane, K., Wu, X., and Chen, J. (2002) A DNA damage-regulated BRCT-containing protein, TopBP1, is required for cell survival, *Mol. Cell. Biol. 22*, 555−566.

13. Liu, K., Lin, F. T., Ruppert, J. M., and Lin, W. C. (2003) Regulation of E2F1 by BRCT domain-containing protein TopBP1, *Mol. Cell. Biol. 23*, 3287−3304.
14. Abbott, D. W., Thompson, M. E., Robinson-Benion, C., Tomlinson, G., Jensen, R. A., and Holt, J. T. (1999) *BRCA1* expression restores radiation resistance in *BRCA1*-defective cancer cells through enhancement of transcription-coupled DNA repair, *J. Biol. Chem. 274*, 18808−18812.
15. Cantor, S. B., Bell, D. W., Ganesan, S., Kass, E. M., Drapkin, R., Grossman, S., Wahrer, D. C., Sgroi, D. C., Lane, W. S., Haber, D. A., and Livingston, D. M. (2001) BACH1, a novel helicase-like protein, interacts directly with BRCA1 and contributes to its DNA repair function, *Cell 105*, 149−160.
16. Yarden, R. I., Pardo-Reoyo, S., Sgagias, M., Cowan, K. H., and Brody, L. C. (2002) BRCA1 regulates the G2/M checkpoint by activating Chk1 kinase upon DNA damage, *Nat. Genet. 30*, 285−289.
17. Gowen, L. C., Avrutskaya, A. V., Latour, A. M., Koller, B. H., and Leadon, S. A. (1998) BRCA1 required for transcription-coupled repair of oxidative DNA damage, *Science 281*, 1009−1012.
18. Harkin, D. P., Bean, J. M., Miklos, D., Song, Y. H., Truong, V. B., Englert, C., Christians, F. C., Ellisen, L. W., Maheswaran, S., Oliner, J. D., and Haber, D. A. (1999) Induction of *GADD45* and JNK/SAPK-dependent apoptosis following inducible expression of *BRCA1*, *Cell 97*, 575−586.
19. Somasundaram, K., Zhang, H., Zeng, Y. X., Houvras, Y., Peng, Y., Zhang, H., Wu, G. S., Licht, J. D., Weber, B. L., and El-Deiry, W. S. (1997) Arrest of the cell cycle by the tumour suppressor BRCA1 requires the CDK-inhibitor $p21^{WAF1/CiPl}$, *Nature 389*, 187−190.
20. Hohenstein, P., Kielman, M. F., Breukel, C., Bennett, L. M., Wiseman, R., Krimpenfort, P., Cornelisse, C., van Ommen, G. J., Devilee, P., and Fodde, R. (2001) A targeted mouse Brca1 mutation removing the last BRCT repeat results in apoptosis and embryonic lethality at the headfold stage, *Oncogene 20*, 2544−2550.
21. Ludwig, T., Fisher, P., Ganesan, S., and Efstratiadis, A. (2001) Tumorigenesis in mice carrying a truncating Brca1 mutation, *Genes Dev. 15*, 1188−1193.
22. Ye, Q., Hu, Y. F., Zhong, H., Nye, A. C., Belmont, A. S., and Li, R. (2001) BRCA1-induced large-scale chromatin unfolding and allele-specific effects of cancer-predisposing mutations, *J. Cell Biol. 155*, 911−921.
23. Chapman, M. S., and Verma, I. M. (1996) Transcriptional activation by BRCA1, *Nature 382*, 678−679.
24. Monteiro, A. N., August, A., and Hanafusa, H. (1996) Evidence for a transcriptional activation function of BRCA1 C-terminal region, *Proc. Natl. Acad. Sci. U.S.A. 93*, 13595−13599.
25. Monteiro, A. N. (2000) BRCA1: exploring the links to transcription, *Trends Biochem. Sci. 25*, 469−474.
26. Miyake, T., Hu, Y. F., Yu, D. S., and Li, R. (2000) A functional comparison of BRCA1 C-terminal domains in transcription activation and chromatin remodeling, *J. Biol. Chem. 275*, 40169−40173.
27. Welcsh, P. L., Lee, M. K., Gonzalez-Hernandez, R. M., Black, D. J., Mahadevappa, M., Swisher, E. M., Warrington, J. A., and King, M. C. (2002) BRCA1 transcriptionally regulates genes involved in breast tumorigenesis, *Proc. Natl. Acad. Sci. U.S.A. 99*, 7560−7565.
28. Ouchi, T., Monteiro, A. N., August, A., Aaronson, S. A., and Hanafusa, H. (1998) BRCA1 regulates p53-dependent gene expression, *Proc. Natl. Acad. Sci. U.S.A. 95*, 2302−2306.
29. Chai, Y. L., Cui, J., Shao, N., Shyam, E., Reddy, P., and Rao, V. N. (1999) The second BRCT domain of BRCA1 proteins interacts with p53 and stimulates transcription from the $p21^{WAF1/CiPl}$ promoter, *Oncogene 18*, 263−268.
30. Hayes, F., Cayanan, C., Barilla, D., and Monteiro, A. N. (2000) Functional assay for BRCA1: mutagenesis of the COOH-terminal region reveals critical residues for transcription activation, *Cancer Res. 60*, 2411−2418.
31. Williams, R. S., Chasman, D. I., Hau, D. D., Hui, B., Lau, A. Y., and Glover, J. N. (2003) Detection of protein folding defects caused by BRCA1-BRCT truncation and missense mutations, *J. Biol. Chem. 278*, 53007−53016.
32. Friedman, L. S., Ostermeyer, E. A., Szabo, C. I., Dowd, P., Lynch, E. D., Rowell, S. E., and King, M. C. (1994) Confirmation of BRCA1 by analysis of germline mutations linked to breast and ovarian cancer in ten families, *Nat. Genet. 8*, 399−404.
33. Miki, Y., Swensen, J., Shattuck-Eidens, D., Futreal, P. A., Harshman, K., Tavtigian, S., Liu, Q., Cochran, C., Bennett, L. M., Ding, W., et al. (1994) A strong candidate for the breast and ovarian cancer susceptibility gene *BRCA1*, *Science 266*, 66−71.
34. Futreal, P. A., Liu, Q., Shattuck-Eidens, D., Cochran, C., Harshman, K., Tavtigian, S., Bennett, L. M., Haugen-Strano, A., Swensen, J., Miki, Y., et al. (1994) *BRCA1* mutations in primary breast and ovarian carcinomas, *Science 266*, 120−122.
35. Breast Cancer Information Core (BIC), http://research.nhgri.nih.gov/bic/.
36. Yarden, R. I., and Brody, L. C. (1999) BRCA1 interacts with components of the histone deacetylase complex, *Proc. Natl. Acad. Sci. U.S.A. 96*, 4983−4988.
37. Yu, X., Wu, L. C., Bowcock, A. M., Aronheim, A., and Baer, R. (1998) The C-terminal (BRCT) domains of BRCA1 interact *in vivo* with CtIP, a protein implicated in the CtBP pathway of transcriptional repression, *J. Biol. Chem. 273*, 25388−25392.
38. Li, S., Chen, P. L., Subramanian, T., Chinnadurai, G., Tomlinson, G., Osborne, C. K., Sharp, Z. D., and Lee, W. H. (1999) Binding of CtIP to the BRCT repeats of BRCA1 involved in the transcription regulation of p21 is disrupted upon DNA damage, *J. Biol. Chem. 274*, 11334−11338.
39. Yamane, K., Katayama, E., and Tsuruo, T. (2000) The BRCT regions of tumor suppressor BRCA1 and of XRCC1 show DNA end binding activity with a multimerizing feature, *Biochem. Biophys. Res. Commun. 279*, 678−684.
40. Zhang, H., Somasundaram, K., Peng, Y., Tian, H., Bi, D., Weber, B. L., and El-Deiry, W. S. (1998) BRCA1 physically associates with p53 and stimulates its transcriptional activity, *Oncogene 16*, 1713−1721.
41. Manke, I. A., Lowery, D. M., Nguyen, A., and Yaffe, M. B. (2003) BRCT repeats as phosphopeptide-binding modules involved in protein targeting, *Science 302*, 636−639.
42. Rodriguez, M., Yu, X., Chen, J., and Songyang, Z. (2003) Phosphopeptide binding specificities of BRCA1 COOH-terminal (BRCT) domains, *J. Biol. Chem. 278*, 52914−52918.
43. Yu, X., Chini, C. C., He, M., Mer, G., and Chen, J. (2003) The BRCT domain is a phospho-protein binding domain, *Science 302*, 639−642.
44. Williams, R. S., Green, R., and Glover, J. N. (2001) Crystal structure of the BRCT repeat region from the breast cancer-associated protein BRCA1, *Nat. Struct. Biol. 8*, 838−842.
45. Joo, W. S., Jeffrey, P. D., Cantor, S. B., Finnin, M. S., Livingston, D. M., and Pavletich, N. P. (2002) Structure of the 53BP1 BRCT region bound to p53 and its comparison to the Brca1 BRCT structure, *Genes Dev. 16*, 583−593.
46. Derbyshire, D. J., Basu, B. P., Serpell, L. C., Joo, W. S., Date, T., Iwabuchi, K., and Doherty, A. J. (2002) Crystal structure of the human 53BP1 BRCT domains bound to p53 tumour suppressor, *EMBO J. 21*, 3863−3872.
47. Zhang, X., Moréra, S., Bates, P. A., Whitehead, P. C., Coffer, A. I., Hainbucher, K., Nash, R. A., Sternberg, M. J., Lindahl, T., and Freemont, P. S. (1998) Structure of an XRCC1 BRCT domain: a new protein−protein interaction module, *EMBO J. 17*, 6404−6411.
48. Krishnan, V. V., Thornton, K. H., Thelen, M. P., and Cosman, M. (2001) Solution structure and backbone dynamics of the human DNA liganse IIIα BRCT domain, *Biochemistry 40*, 13158−13166.
49. Lee, J. Y., Chang, C., Song, H. K., Moon, J., Yang, J. K., Kim, H. K., Kwon, S. T., and Suh, S. W. (2000) Crystal Structure of NAD^+-dependent DNA ligase: modular architecture and functional implications, *Embo J. 19*, 1119−1129.
50. Shiozaki, E. N., Gu, L., Yan, N., and Shi, Y. (2004) Structure of the BRCT repeats of BRCA1 bound to a BACH1 phosphopeptide: implications for signaling, *Mol. Cell 14*, 405−412.
51. Clapperton, J. A., Manke, I. A., Lowery, D. M., Ho, T., Haire, L. F., Yaffe, M. B., and Smerdon, S. J. (2004) Structure and mechanism of BRCA1 BRCT domain recognition of phosphorylated BACH1 with implications for cancer, *Nat. Struct. Mol. Biol. 11*, 512−518.
52. Williams, R. S., Lee, M. S., Hau, D. D., and Glover, J. N. (2004) Structural basis of phosphopeptide recognition by the BRCT domain of BRCA1, *Nat. Struct. Mol. Biol. 11*, 519−525.
53. Neidhardt, F. C., Bloch, P. L., and Smith, D. F. (1974) Culture medium for enterobacteria, *J. Bacteriol. 119*, 736−747.
54. Kanelis, V., Forman-Kay, J. D., and Kay, L. E. (2001) Multidimensional NMR methods for protein structure determination, *IUBMB Life 52*, 291−302.

55. Goddard, T. D., and Kneller, D. G. (2003) *SPARKY 3*, University of California, San Francisco.
56. Ball, L. J., Kühne, R., Hoffmann, B., Hafner, A., Schmieder, P., Volkmer-Engert, R., Hof, M., Wahl, M., Schneider-Mergener, J., Walter, U., Oschkinat, H., and Jarchau, T. (2000) Dual epitope recognition by the VASP EVH1 domain modulates polyproline ligand specificity and binding affinity, *EMBO J. 19*, 4903−4914.
57. Kraulis, P. (1989) ANSIG: a program for the assignment of protein ^{1}H 2D NMR spectra by interactive graphics, *J. Magn. Reson. 24*, 627−633.
58. Brunger, A. T., Adams, P. D., Clore, G. M., DeLano, W. L., Gros, P., Grosse-Kunstleve, R. W., Jiang, J. S., Kuszewski, J., Nilges, M., Pannu, N. S., Read, R. J., Rice, L. M., Simonson, T., and Warren, G. L. (1998) Crystallography and NMR system: a new software suite for macromolecular structure determination, *Acta Crystallogr. D54*, 905−921.
59. Billeter, M., Neri, D., Otting, G., Qian, Y. Q., and Wuthrich, K. (1992) Precise vicinal coupling constants ^{3}JHNα in proteins from nonlinear fits of J-modulated [^{15}N-^{1}H]-COSY experiments, *J. Biomol. NMR 2*, 257−274.
60. Zamyatnin, A. A. (1972) Protein volume in solution, *Prog. Biophys. Mol. Biol. 24*, 107−123.
61. Zamyatnin, A. A. (1984) Amino acid, peptide, and protein volume in solution, *Annu. Rev. Biophys. Bioeng. 13*, 145−165.
62. Lamm, O. (1929) Die Differentialgleichung der Ultrazentrifugierung, *Ark. Mat., Astron. Fys. 21B*, 1−4.
63. Schuck, P. (1998) Sedimentation analysis of noninteracting and self-associating solutes using numerical solutions to the Lamm equation, *Biophys. J. 75*, 1503−1512.
64. Behlke, J., and Ristau, O. (1997) Molecular mass determination by sedimentation velocity experiments and direct fitting of the concentration profiles, *Biophys. J. 72*, 428−434.
65. Behlke, J., and Ristau, O. (2002) A new approximate whole boundary solution of the Lamm differential equation for the analysis of sedimentation velocity experiments, *Biophys. Chem. 95*, 59−68.
66. Van Holde, K. E., and Weischet, W. O. (1978) Boundary analysis of sedimentation velocity experiments with monodisperse and paucidisperse solutes, *Biopolymers 17*, 1387−1403.
67. Demeler, B., Saber, H., and Hansen, J. C. (1997) Identification and interpretation of complexity in sedimentation velocity boundaries, *Biophys. J. 72*, 397−407.
68. Gill, S. C., and von Hippel, P. H. (1989) Calculation of protein extinction coefficients from amino acid sequence data, *Anal. Biochem. 182*, 319−326.
69. Johnson, M. L., Correia, J. J., Yphantis, D. A., and Halvorson, H. R. (1981) Analysis of data from the analytical ultracentrifuge by nonlinear least-squares techniques, *Biophys. J. 36*, 575−588.
70. McRorie, D. K., and Voelker, P. J. (1993) *Self-Associating Systems in the Analytical Ultracentrifuge*, Beckman Instruments, Inc., Fullerton, CA.
71. Williams, R. S., and Glover, J. N. (2003) Structural consequences of a cancer-causing BRCA1-BRCT missense mutation, *J. Biol. Chem. 278*, 2630−2635.
72. Koonin, E. V., Wolf, Y. I., and Karev, G. P. (2002) The structure of the protein universe and genome evolution, *Nature 420*, 218−223.
73. Laskowski, R. A., Rullmannn, J. A., MacArthur, M. W., Kaptein, R., and Thornton, J. M. (1996) AQUA and PROCHECK-NMR: programs for checking the quality of protein structures solved by NMR, *J. Biomol. NMR 8*, 477−486.
74. Koradi, R., Billeter, M., and Wüthrich, K. (1996) MOLMOL: a program for display and analysis of macromolecular structures, *J. Mol. Graphics 14*, 51−55.

BI049550Q